Inorganic Chemistry

Article

pubs.acs.org/IC

Control of Intramolecular $\pi-\pi$ Stacking Interaction in Cationic Iridium Complexes via Fluorination of Pendant Phenyl Rings

Lei He, Dongxin Ma, Lian Duan,* Yongge Wei, Juan Qiao, Deqiang Zhang, Guifang Dong, Liduo Wang, and Yong Qiu*

Key Laboratory of Organic Optoelectronics and Molecular Engineering, Ministry of Education, Department of Chemistry, Tsinghua University, Beijing 100084, P.R. China

Supporting Information

ABSTRACT: Intramolecular $\pi-\pi$ stacking interaction in one kind of phosphorescent cationic iridium complexes has been controlled through fluorination of the pendant phenyl rings on the ancillary ligands. Two blue-green-emitting cationic iridium complexes, $[Ir(ppy)_2(F2phpzpy)]PF_6$ (**2**) and $[Ir(ppy)_2(F5phpzpy)]PF_6$ (**3**), with the pendant phenyl rings on the ancillary ligands substituted with two and five fluorine atoms, respectively, have been synthesized and compared to the parent complex, $[Ir(ppy)_2(phpzpy)]PF_6$ (**1**). Here Hppy is 2-phenylpyridine, F2phpzpy is 2-(1-(3,5-difluorophenyl)-1*H*-pyrazol-3-yl)pyridine, F5phpzpy is 2-(1-pentafluorophenyl-1*H*-pyrazol-3-yl)-pyridine, and phpzpy is 2-(1-phenyl-1*H*-pyrazol-3-yl)pyridine. Single crystal structures reveal that the pendant phenyl rings on the ancillary ligands stack to the phenyl rings of the ppy ligands, with dihedral angles of 21°, 18°, and 5.0° between least-squares planes for complexes **1**, **2**, and **3**, respectively, and centroid-centroid distances of 3.75, 3.65, and 3.52 Å for complexes **1**, **2**, and **3**, respectively, indicating progressively reinforced intramolecular $\pi-\pi$ stacking interactions from complexes **1** to **2** and **3**. Compared to complex **1**, complex **3** with a significantly reinforced intramolecular face-to-face $\pi-\pi$ stacking interaction exhibits a significantly enhanced (by 1 order of magnitude) photoluminescent efficiency in solution. Theoretical calculations reveal that in complex **3** it is unfavorable in energy for the pentafluorophenyl ring to swing by a large degree and the intramolecular $\pi-\pi$ stacking interaction remains on the lowest triplet state.

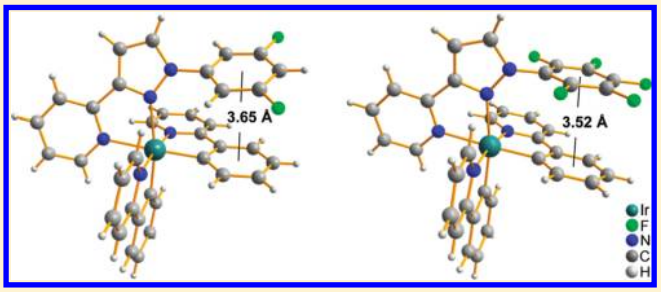

INTRODUCTION

Phosphorescent cationic iridium complexes have been widely used in biological-labeling, oxygen or ion-sensing, and organic electroluminescent devices, including light-emitting electrochemical cells[1−4] and organic light-emitting diodes.[5−7] Typical phosphorescent cationic iridium complexes use 2-phenylpyridine (Hppy) as the cyclometalated ligands and 2,2′-bipyridine (bpy) as the ancillary ligands, and give orange-red light emission.[3,4] To enhance the luminescent efficiency and tune the emission color, various cationic iridium complexes have been developed with tailored ligands.[4,8−15] Through attaching phenyl rings at the 6 positions of the bpy ancillary ligands, intramolecular $\pi-\pi$ stacking interactions have been introduced into the complexes.[16−21,47] Within the complexes, the attached pendant phenyl rings stack to the phenyl rings of the ppy ligands. For phenyl−phenyl $\pi-\pi$ stacking interactions, generally there exist three stacking patterns: face-to-face (sandwich), edge-to-face (T-shaped), and offset face-to-face (parallel-displaced).[22,23] The latter two are stable in energy, while the face-to-face stacking is unstable and rarely observed because of the repulsion between the two stacking phenyl rings. For reported cationic iridium complexes, the introduced intramolecular phenyl−phenyl $\pi-\pi$ stacking generally adopts an energetically favorable offset face-to-face pattern.[18,20] However, for these complexes, introduction of the intramolecular $\pi-\pi$ stacking interaction generally results in large configurational distortions of the bpy ancillary ligands, which significantly decreases the photoluminescent (PL) efficiencies of the complexes.[18,24]

Recently, we reported a blue-green-emitting cationic iridium complex, $[Ir(ppy)_2(phpzpy)]PF_6$ (complex **1**, Scheme 1), with 2-(1-phenyl-1*H*-pyrazol-3-yl) pyridine (phpzpy) as the ancillary ligand.[25] Because of the pyrazole-type ancillary ligand used,[9,25] complex **1** shows an enlarged energy gap and significantly blue-shifted emission compared to the typical complex $[Ir(ppy)_2(bpy)]PF_6$. The pendant phenyl ring on phpzpy stacks to the phenyl ring of the ppy ligand, with a dihedral angle of 21° between the least-squares planes and a centroid-centroid distance of 3.75 Å.[25] The phenyl−phenyl stacking in complex **1** is far from parallel and shows a relatively large centroid-centroid distance, largely because of the repulsion between the two stacking phenyl rings.[22] In the present work, we aim to control the intramolecular $\pi-\pi$ stacking interaction in the archetype complex **1**. The approach is to fluorinate the pendant phenyl ring. The basis for this molecular design is that quadrupole

Received: October 2, 2011
Published: March 30, 2012

ACS Publications © 2012 American Chemical Society

dx.doi.org/10.1021/ic2021325 | *Inorg. Chem.* 2012, 51, 4502−4510

Scheme 1. Molecular Structures of Complexes 1−3

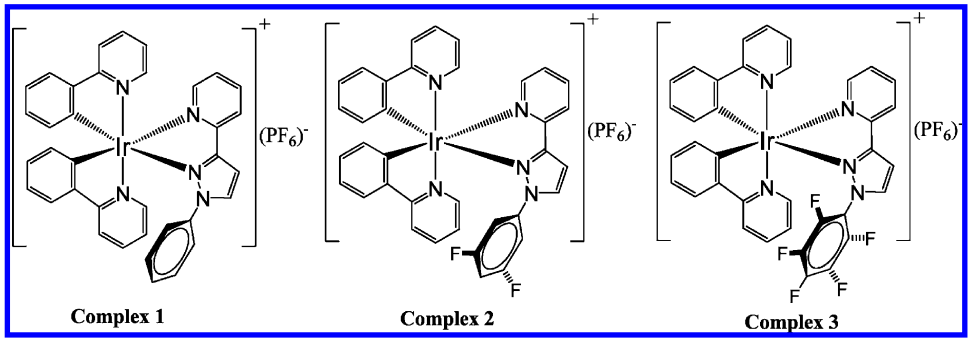

moments of benzene and hexafluorobenzene are opposite in sign because of the electronegativity of fluorine atoms.[26] Benzene dimers generally stack with each other in an offset face-to-face or edge-to-face manner to minimize the repulsion between the two stacking benzenes,[27] while in the crystal of 1:1 mixture of benzene and hexafluorobenzene, benzene and hexafluorobenzene stacks alternately to each other in a parallel face-to-face manner rather than an offset face-to-face or edge-to-face manner, because of the strong electrostatic attraction between benzene and hexafluorobenzene.[27,28] By taking advantage of this ordered parallel stacking, fluorine-substituted aryls have been widely used as motifs in supramolecular chemistry[29] and organic semiconductors.[30,31]

To reinforce the intramolecular $\pi-\pi$ stacking interaction, the pendant phenyl ring in complex **1** is substituted with fluorine atoms, yielding complexes **2** and **3** (Scheme 1), of which the pendant phenyl rings are substituted with two and five fluorine atoms, respectively. Single crystal structures reveal that, upon fluorination, the pendant phenyl rings stack more parallel and closer to the phenyl rings of the ppy ligands, with complex **3** exhibiting a significantly reinforced intramolecular $\pi-\pi$ stacking interaction. In complex **3**, the pentafluorophenyl−phenyl stacking fits better a face-to-face pattern rather than an offset face-to-face pattern. Moreover, introduction of the intramolecular $\pi-\pi$ stacking interaction in complex **3** results in little distortion of the ligands. Compared to complex **1**, complex **3** shows a significantly enhanced (by 1 order of magnitude) PL efficiency in solution.

Theoretical calculations revealed that, in complex **3**, it is unfavorable in energy for the pendant pentafluorophenyl ring to swing by a large degree. While in complexes **1** and **2**, the pendant phenyl or 3,5-difluorophenyl rings can swing by a relatively larger degree. For complex **3**, the intramolecular $\pi-\pi$ stacking interaction remains on the lowest triplet state. Among the three complexes, complex **3** exhibits the smallest structural deviations between the ground and the lowest triplet states.

EXPERIMENTAL SECTION

General Procedures. All reactants and solvents were purchased from commercial sources and, unless otherwise stated, used as received. Mass spectrometry was performed with a Thermo Electron Corporation Finnigan LTQ mass spectrometer. NMR spectra were recorded on a JEOL JNM-ECA600 NMR spectrometer. Elemental analysis was determined with an Elementar Vario EL CHN elemental analyzer. Absorption spectra were recorded with an Agilent 8453 UV−vis spectrophotometer. PL spectra were recorded with a fluorospectrophotometer (Jobin Yvon, FluoroMax-3). The PL transient lifetimes were measured on a transient spectrofluorimeter (Edinburgh Instruments, FLSP920). The photoluminescent quantum yields (PLQYs) were measured in degassed CH_3CN solution versus quinine sulfate (Φ_p = 0.545 in 1 M H_2SO_4).[32] The PLQYs in thin films were measured with an integrating sphere on a fluorospectrophotometer (Jobin Yvon, FluoroMax-3) according to a reported procedure.[33]

Synthesis. *Synthesis of 2-(1-(3,5-Difluorophenyl)-1H-pyrazol-3-yl)pyridine (F2phpzpy).* 2-(1*H*-pyrazol-3-yl)pyridine (0.58 g, 4 mmol), 1,3,5-trifluorobenzene (2.6 g, 19 mmol) and K_2CO_3 (1.1 g, 8 mmol) were dissolved in dimethylsulfoxide (20 mL). The mixture was refluxed at 110 °C for 5 h, cooled to room temperature, and extracted with CH_2Cl_2 (100 mL). The organic layer was separated, washed with brine, dried over Na_2SO_4, and purified by column chromatography on silica gel (200−300 mesh) with petroleum ether/ethyl acetate (15:1) as the eluent, yielding a white solid (0.85 g, 3.3 mmol). Yield: 83%. ^{1}H NMR (chloroform-d_6, 600 MHz, δ[ppm]): 8.66(d, J = 4.1 Hz, 1H), 8.12(d, J = 8.2 Hz, 1H), 7.97(d, J = 2.8 Hz, 1H), 7.78(td, J = 7.6 and 2.0 Hz, 1H), 7.41−7.35 (m, 2H),7.30−7.27(m, 1H), 7.17(d, J = 2.8 Hz, 1H), 6.75(tt, J = 8.6 and 2.4 Hz, 1H). ^{13}C NMR (chloroform-d_6, 150 MHz, δ[ppm]): 163.62(dd, $^1J_{CF}$ = 247.0 Hz, $^3J_{CF}$ = 14.4 Hz), 154.02, 151.47, 149.55, 142.00(t, $^3J_{CF}$ = 12.9 Hz), 136.78, 128.29, 123.18, 120.54, 107.52, (dd, $^2J_{CF}$ = 23.0 Hz, $^4J_{CF}$ = 7.2 Hz), 101.67(t, $^2J_{CF}$ = 25.1 Hz). ESI-MS [m/z]: 258.1 $[M+H]^+$.

Synthesis of 2-(1-Pentafluorophenyl-1H-pyrazol-3-yl)-pyridine (F5phpzpy). 2-(1*H*-pyrazol-3-yl)pyridine (0.7 g, 4.8 mmol), perfluorobenzene (8.1 g, 43 mmol), and K_2CO_3 (1.4 g, 10 mmol) were dissolved in dimethylsulfoxide (30 mL). The mixture was refluxed at 110 °C for 6 h, cooled to room temperature, and extracted with CH_2Cl_2 (100 mL). The organic layer was separated, washed with brine, dried over Na_2SO_4, and purified by column chromatography on silica gel (200−300 mesh) with petroleum ether/ethyl acetate (15:1) as the eluent, yielding a white solid (0.51 g, 1.6 mmol). Yield: 33%. ^{1}H NMR (acetone-d_6, 600 MHz, δ[ppm]): 8.65(d, J = 4.8 Hz, 1H), 8.14(s, 1H), 8.07(d, J = 8.2 Hz, 1H), 7.87(td, J = 7.6 and 1.4 Hz, 1H), 7.37(td, J = 6.3 and 1.1 Hz, 1H), 7.23(d, J = 2.7 Hz, 1H). ^{13}C NMR (acetone-d_6, 150 MHz, δ[ppm]): 155.04, 151.33, 149.58, 144.20−143.97(m), 142.50−142.10(m), 140.70−140.40(m), 139.13−138.84(m), 137.50−137.20(m), 136.71, 134.70, 123.33, 116.82−116.55(m), 119.90, 106.50. ESI-MS [m/z]: 312.13 $[M+H]^+$.

Synthesis of [Ir(ppy)$_2$(F2phpzpy)]PF$_6$ (Complex 2). The dichloro-bridged diiridium complex $[Ir(ppy)_2Cl]_2$ (0.46 g, 0.43 mmol) and F2phpzpy (0.23 g, 0.9 mmol) were suspended in ethane-1,2-diol (20 mL). The mixture was refluxed at 130 °C for 13 h under Ar atmosphere, cooled to room temperature and diluted with deionized water (100 mL). To the solution, NH_4PF_6 (1.4 g, 8.6 mmol) in deionized water (20 mL) was slowly added under stirring, resulting in a yellow suspension. The suspension was filtered and the precipitate was dried under vacuum at 70 °C for 5 h. The crude product was purified by column chromatography on silica gel (200−300 mesh) with CH_2Cl_2/acetone (50:1) as the eluent, yielding a yellow solid (0.52 g, 0.55 mmol). Yield: 64%. ^{1}H NMR (acetone-d_6, 600 MHz, δ[ppm]): 8.55(d, J = 8.2 Hz, 1H), 8.29(d, J = 2.8 Hz, 1H), 8.22(td, J = 7.9 and 2.1 Hz, 1H), 8.19(d, J = 8.2 Hz, 1H), 8.16(d, J = 8.3 Hz, 1H), 8.14(d, J = 5.5 Hz, 1H), 8.04(td, J = 8.0 and 1.4 Hz, 1H), 7.99−7.92(m, 2H), 7.88(d, J = 7.6 Hz, 1H), 7.77(d, J = 7.9 Hz, 1H), 7.68(d, J = 2,8 Hz, 1H), 7.60(d, J = 7.6 Hz, 1H), 7.54(td, J = 6.5 and 1.4 Hz,

dx.doi.org/10.1021/ic2021325 | Inorg. Chem. 2012, 51, 4502−4510

Scheme 2. Synthesis of the Ancillary Ligands and Complexes 2 and 3

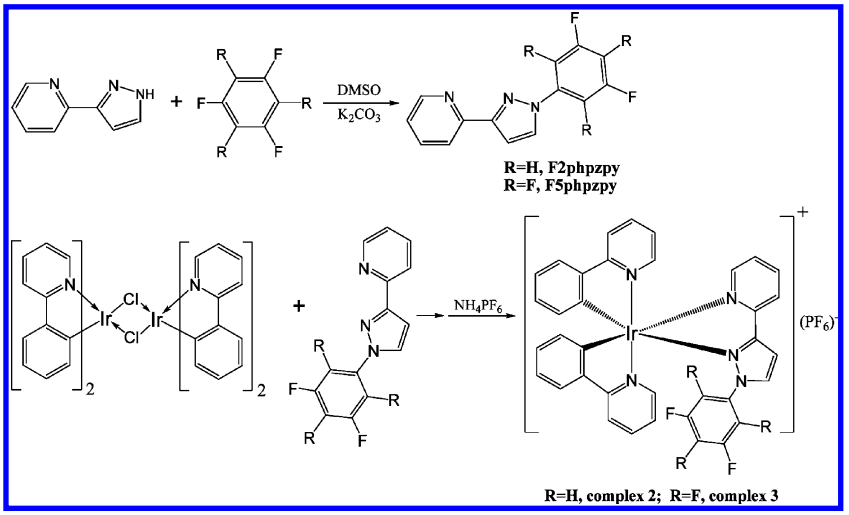

1H), 7.29(td, J = 6.5 and 1.3 Hz, 1H), 7.23(td, J = 6.5 and 1.3 Hz, 1H), 6.97(t, J = 7.6 Hz, 1H), 6.85(t, J = 7.6 Hz, 1H), 6.82−6.76(m, 3H), 6.69(t, J = 7.6 Hz, 1H), 6.52(t, J = 8.2 Hz, 1H), 6.14(d, J = 6.8 Hz, 1H), 5.91(d, J = 7.6 Hz, 1H). ^{13}C NMR (acetone-d_6, 150 MHz, δ[ppm]): 168.20, 167.19, 161.81(dd, $^1J_{CF}$ = 247 Hz, $^3J_{CF}$ = 14.4 Hz), 154.87, 151.54, 150.27, 150.14, 149.87, 147.91, 146.73, 144.12, 143.94, 139.86, 139.00(t, $^3J_{CF}$ = 12.9 Hz), 138.76, 137.98, 131.55, 130.87, 130.42, 129.23, 127.05, 124.82, 124.20, 124.04, 123.70, 123.36, 122.78, 121.70, 119.91, 119.64, 110.92(dd, $^2J_{CF}$ = 21.5 Hz, $^4J_{CF}$ = 7.2 Hz), 107.39, 106.39(t, $^2J_{CF}$ = 25.1 Hz). ESI-MS [m/z]: 758.3 [M − PF_6]$^+$. Anal. Found: C, 47.94; H, 2.96; N, 7.65. Anal. Calcd. for $C_{36}H_{25}F_8N_5PIr$: C, 47.90; H, 2.79; N, 7.76.

Synthesis of [Ir(ppy)$_2$(F5phpzpy)]PF$_6$ (Complex 3). The synthesis of complex **3** is similar to that of complex **2**, except that F2phpzpy was replaced with F5phpzpy. Yield: 67%. ^{1}H NMR (acetone-d_6, 600 MHz, δ[ppm]): 8.63(d, J = 8.3 Hz, 1H), 8.43(d, J = 3.4 Hz, 1H), 8.27(td, J = 8.2 and 1.4 Hz, 1H), 8.24(d, J = 8.2 Hz, 1H), 8.20(d, J = 8.3 Hz, 1H), 8.07(td, J = 7.9 and 1.4 Hz, 1H), 8.02−7.98(m, 2H), 7.96(d, J = 5.4 Hz, 1H), 7.90(d, J = 5.5 Hz, 1H), 7.85(d, J = 2.8 Hz, 1H), 7.81(d, J = 8.2 Hz, 1H), 7.70(d, J = 8.3 Hz, 1H), 7.60(td, J = 6.5 and 1.4 Hz, 1H), 7.34(td, J = 6.5 and 1.4 Hz, 1H), 7.25(td, J = 6.5 and 1.4 Hz, 1H), 7.00(td, J = 7.6 and 1.4 Hz, 1H), 6.86(td, J = 7.6 and 1.4 Hz, 1H), 6.83(t, J = 8.3 Hz, 1H), 6.69(t, J = 6.9 Hz, 1H), 6.14(d, J = 7.6 Hz, 1H), 6.09(d, J = 7.6 Hz, 1H). ^{13}C NMR (DMSO-d_6, 150 MHz, δ[ppm]): 167.23, 166.74, 156.22, 150.61, 150.22, 150.05, 149.66, 147.46, 147.20, 145.30−144.70(m), 144.42, 144.25, 143.60−143.10(m), 141.75−141.40(m), 140.78, 140.65, 139.66, 139.57, 137.75−137.00(m), 136.10−135.40(m), 131.36, 130.92, 130.79, 129.59, 128.24, 125.56, 124.98, 124.55, 123.31, 121.61, 120.75, 120.16, 113.30−113.00(m), 109.18. ESI-MS [m/z]: 812.22 [M − PF_6]$^+$. Anal. Found: C, 45.29; H, 2.46; N, 7.16. Anal. Calcd. for $C_{36}H_{22}F_{11}N_5PIr$: C, 45.19; H, 2.32; N, 7.32.

Crystal Structure Determination. The low temperature (153.15 K) single-crystal X-ray experiments were performed on a Rigaku CCD Saturn 724+ diffractometer equipped with graphite monochromatized Mo Kα radiation. Direct phase determination yielded the positions of all non-hydrogen atoms which were subjected to anisotropic refinement. All hydrogen atoms were generated theoretically and rode on their parent atoms in the final refinement.

Theoretical Calculations. Density functional theory (DFT) and time-dependent DFT (TD-DFT) at the spin-restricted B3LYP level were adopted for calculations on the ground and excited electronic states of the complexes.[34−36] "Double-ξ" quality basis sets were employed for the C, H, N, F (6-31G**)[37] and the Ir (LANL2DZ).[38] An effective core potential (ECP) replaces the inner core electrons of Ir leaving the outer core $(5s)^2(5p)^6$ electrons and the $(5d)^6$ valence electrons of Ir(III).[38] The geometry of the singlet ground state (S_0) was fully optimized with a C1 symmetry constraint. The lowest triplet states (T_1) were optimized at the spin-unrestricted B3LYP level with a spin multiplicity of 3 and a C1 symmetry constraint. All calculations were carried out with the Gaussian 03 software package.[39]

RESULTS AND DISCUSSION

Synthesis and Characterizations. Scheme 2 depicts the synthetic routes toward the ancillary ligands 2-(1-(3,5-difluorophenyl)-1*H*-pyrazol-3-yl)pyridine (F2phpzpy) and 2-(1-pentafluorophenyl-1*H*-pyrazol-3-yl)-pyridine (F5phpzpy), and complexes **2** and **3**. F2phpzpy and F5phpzpy were directly synthesized from 2-(1*H*-pyrazol-3-yl)pyridine and fluorobenzene by nucleophilic substitution reactions. To suppress the formation of multisubstitution products, fluorobenzene was in large excess over 2-(1*H*-pyrazol-3-yl)pyridine in the reaction mixture. Complexes **2** and **3** were readily synthesized from the dimeric iridium(III) intermediate [Ir(ppy)$_2$Cl]$_2$ and the ancillary ligands by a conventional synthetic method.[3] All ligands and complexes were fully characterized by ESI (electrospray ionization) mass spectrometry, ^{1}H NMR and ^{13}C NMR spectroscopy. The purity of the complexes was further ensured by elemental analysis.

Single Crystal Structures. Single crystals of complexes **2** and **3** were grown from slow evaporation of acetone/methanol solution. Figure 1 depicts single crystal structures of complexes **2** and **3**. Similar to other cationic iridium complexes,[9,15,25] complexes **2** and **3** exhibit distorted octahedral geometries around the iridium centers, with two ppy ligands adopting *C,C*-cis, *N,N*-trans configurations. Selected bond lengths and angles for complexes **1**−**3** are presented in Table 1. In complex **2**, Ir−N(F2phpzpy) bonds (2.173 and 2.185 Å) are longer than Ir−N(ppy) bonds (2.040 and 2.040 Å), because of the strong trans-influence of Ir−C(ppy) bonds. Similarly, in complex **3**, Ir−N(F5phpzpy) bonds (2.179 and 2.140 Å) are longer than Ir−N(ppy) bonds (2.040 and 2.046 Å). As shown in Table 1, for complexes **1**−**3**, the bond lengths and ligand bite angles around the iridium centers are similar, except that, in complex **3**, the Ir−N(pyrazole) bond length (2.140 Å) is shortened by about 0.04 Å compared to those in complexes **1** and **2** (2.174 and 2.185 Å, respectively).

In typical cationic iridium complexes with intramolecular $\pi-\pi$ stacking interactions, the bpy ancillary ligands generally exhibit configurational distortions, as revealed by large dihedral angles (about 20°) of the two pyridine planes on the bpy

dx.doi.org/10.1021/ic2021325 | *Inorg. Chem.* 2012, 51, 4502−4510

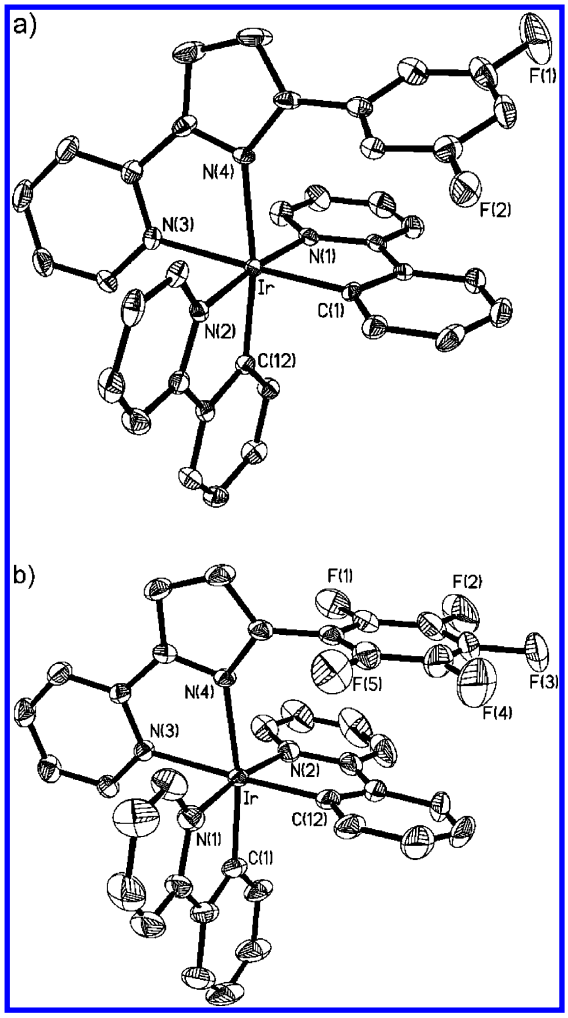

Figure 1. Crystal structures of (a) complex **2** and (b) complex **3**. Thermal ellipsoids are drawn at 35% probability. The PF_6^- counteranions and hydrogen atoms are omitted for clarity.

ligands.[18,24] In complexes **1**, **2**, and **3**, the dihedral angles (φ) of the pyridine and pyrazole planes on the ancillary ligands are 7.2°, 13°, and 4.3°, respectively. For complex **3**, the small φ value indicates that the pyridine-pyrazole skeleton of F5phpzpy is little distorted. While in complex **2**, the relatively large φ value indicates a relatively large configurational distortion for F2phpzpy.

As shown in Figure 1, in complex **2**, the pendant 3,5-difluorophenyl ring stacks to the phenyl ring of the ppy ligand, with a dihedral angle (Φ) of 18° between the least-squares planes and a centroid-centroid distance (d) of 3.65 Å; in complex **3**, the pendant pentafluorophenyl ring stacks parallel to the phenyl ring of the ppy ligand, with a small dihedral angle of 5.0°, a short centroid-centroid distance of 3.52 Å, and a short centroid-to-plane distance of 3.41 Å. As previously reported, in complex **1**, the pendant phenyl ring stacks to the phenyl ring of the ppy ligand, with a large dihedral angle of 21° between least-squares planes and a large centroid-centroid distance of 3.75 Å. Upon fluorinating the pendant phenyl ring, the intramolecular phenyl−phenyl stacking indeed becomes more parallel and closer, indicating progressively reinforced intramolecular $\pi-\pi$ stacking interactions. However, in complex **2**, the stacking of the phenyl and 3,5-difluorophenyl rings is still far from parallel and exhibits a relatively large centroid-centroid distance, indicating a reinforced but still weak intramolecular $\pi-\pi$ stacking interaction. This suggests that substitution of the pendant phenyl ring with two fluorine atoms is insufficient to remarkably change the quadrupole moment of the phenyl ring and significantly reinforce the intramolecular $\pi-\pi$ stacking interaction. In complex **3**, the phenyl-pentafluorophenyl stacking is parallel and close, corresponding to a significantly reinforced $\pi-\pi$ stacking interaction, because of the strong electrostatic attraction between phenyl and pentafluorophenyl rings.[27,28] As observed in the single crystal structure, the $\pi-\pi$ stacking in complex **3** fits better a face-to-face pattern rather than an offset face-to-face pattern.

Photophysical Properties. Figure 2 depicts the absorption and PL spectra of complexes **2** and **3** in CH_3CN solution and as neat films. Detailed photophysical characteristics are summarized in Tables 2 and 3. As a comparison, the data of complex **1** are also listed. The absorption spectra of complexes **2** and **3** have characteristics of the absorption spectra of phosphorescent iridium complexes, with the intense absorption bands in the ultraviolet region (below 350 nm) assigned to $^1\pi-\pi^*$ transitions of the ligands and the relatively weak absorption bands extending to the visible region assigned to ^{1}MLCT (metal-to-ligand charge-transfer), ^{1}LLCT (ligand-to-ligand charge-transfer), ^{3}MLCT, ^{3}LLCT, and ligand-centered $^3\pi-\pi^*$ transitions.[9,11,13−15]

Similar to complex **1**,[25] in CH_3CN solution, complexes **2** and **3** emit blue-green light with emission maxima at 480 and 476 nm, respectively. The fluorination on the pendant phenyl ring exerts little influence on the emission energy of the complexes. Complexes **1**−**3** all show significantly blue-shifted light emission as compared to the typical complex $[Ir(bpy)_2(ppy)]$-PF_6 (PL = 585 nm), because of pyrazole-type ancillary ligands used.[9,25] As shown in Figure 2, at 77 K in CH_3CN glass, the emission spectra of complexes **2** and **3** are little blue-shifted as compared to their emission spectra at room temperature. This,

Table 1. Selected Bond Lengths (Å) and Angles (deg) in Single Crystal Structures of Complexes 1−3

	metal−ligand bond lengths			ligand bite angles				
	Ir−C(ppy)	Ir−N(ppy)	Ir−N(N∧N)[b]	ppy	N∧N	φ[c]	Φ[d]	d[e]
1[a]	2.000(5)	2.050(3)	2.179(4)	80.78(16)	74.61(15)	7.2	21	3.75
	2.015(5)	2.052(3)	2.174(3)	80.04(16)				
2	1.998(4)	2.040(3)	2.173(3)	80.62(13)	75.46(10)	13	18	3.65
	2.010(4)	2.040(3)	2.185(3)	80.18(13)				
3	2.000(6)	2.040(5)	2.179(5)	80.98(25)	74.36(18)	4.3	5.0	3.52
	2.004(6)	2.046(5)	2.140(4)	81.09(25)				

[a]Data of complex **1** were cited from ref 25. [b]N∧N denotes ancillary ligand. [c]Dihedral angle of the pyridine and pyrazole planes on the ancillary ligand. [d]Dihedral angle of the two stacking phenyl rings. [e]Centroid-centroid distance of the two stacking phenyl rings.

dx.doi.org/10.1021/ic2021325 | Inorg. Chem. 2012, 51, 4502−4510

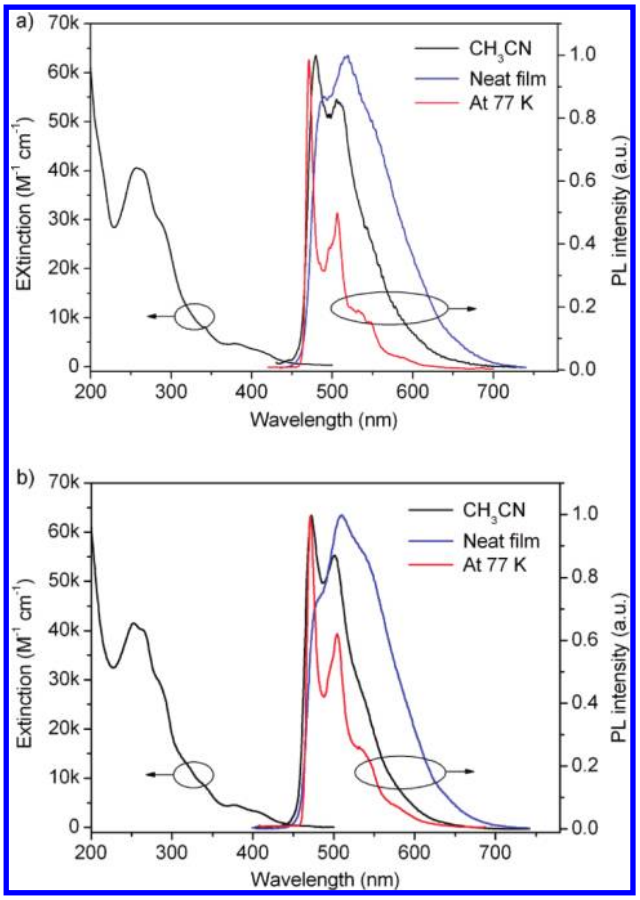

Figure 2. Absorption and PL spectra of (a) complex **2** and (b) complex **3** in CH_3CN solution and as neat films.

together with the structured emission spectra, indicates that the emission of complexes **2** and **3** has strong ligand-centered $^3\pi-\pi^*$ character.[40,41]

In CH_3CN solution, the PLQYs of complexes **1**, **2**, and **3** are 0.03, 0.008, and 0.32, respectively, and the excited-state lifetimes are 0.18, 0.05, and 2.0 μs, respectively. Compared to the parent complex **1**, complex **3** shows significantly increased PLQY and excited-state lifetime, while complex **2** shows decreased PLQY and excited-state lifetime. The radiative (k_r) and nonradiative (k_{nr}) rates of complexes **1**–**3** in CH_3CN solution are calculated and listed in Table 2. The k_r values of complexes **1**–**3** are nearly the same. The k_{nr} value of complex **3** is much smaller than that of complex **1**, while the k_{nr} value of complex **2** is higher than that of complex **1**. For phosphorescent heavy-metal complexes, an important channel for the nonradiative deactivation of the emitting excited-states is the vibrational coupling between the ground and the excited states, which occurs when there are structural changes between the two states.[24] The low k_{nr} value of complex **3** suggests that complex **3** should have much smaller structural changes between the ground and the excited states as compared to complexes **1** and **2**.

Table 3. Photophysical Characteristics of Complexes 1–3 in Thin Films

	5% doped PMMA films			neat films		
	PL λ [nm]	Φ_p	τ [μs]	PL λ [nm]	Φ_p	τ [μs]
1[a]	481, 510	0.84	3.0	486, 513	0.07	0.18 (74%), 0.43 (26%)
2	480, 510	0.59	3.1	519, 490	0.05	0.16 (62%), 0.56 (38%)
3	477, 506	0.78	3.5	516, 484	0.08	0.92 (41%), 0.25 (59%)

[a]Data of complex **1** were cited from ref 25.

As shown in Table 3, in the 5% doped poly(methyl methacrylate) (PMMA) films, complexes **1**–**3** show comparable high PLQYs and long excited-state lifetimes. The PLQYs and excited-state lifetimes in the lightly doped PMMA films are significantly increased compared to those in solution, as always observed for phosphorescent cationic iridium complexes,[9,16] because of restricted intramolecular rotations or vibrations in solid-states.[42–44] It is noted that, in the 5% doped PMMA films, complex **2** still exhibits the lowest PLQY among the three complexes, which suggests that a relatively large structural change still exists between the ground and the excited states for complex **2** in the solid state. In neat films, complexes **1**–**3** all exhibit red-shifted light emission (Supporting Information, Figure S1) and largely decreased PLQYs and excited-state lifetimes, because of the strong intermolecular interactions in close-packed neat films.[45]

In solution, the PLQY of complex **3** is much higher than that of complex **1** and comparable to those of other blue-green-emitting cationic iridium complexes reported,[9,14,15] indicating that introduction of the intramolecular $\pi-\pi$ stacking interaction does not decrease the PL efficiency. This differs from previous reports where complexes with intramolecular phenyl–phenyl $\pi-\pi$ stacking interactions generally show decreased PL efficiencies because of the configurational distortion of the ancillary ligands.[24] Complex **3** with a significantly reinforced intramolecular $\pi-\pi$ stacking interaction and a high luminescent efficiency is an interesting candidate for applications in phosphorescent systems.

Theoretical Calculations. To gain deeper insight into the intramolecular $\pi-\pi$ stacking interaction, quantum chemical calculations on the ground and exited states were performed for complexes **1**–**3**. The ground-state (S_0) structures of complexes **1**–**3** were optimized by DFT calculations. The calculated bond lengths and angles agree well with the experimental X-ray values (Supporting Information, Table S1), except that the Ir–N bonds between the iridium ions and the ancillary ligands are

Table 2. Photophysical Characteristics of Complexes 1–3 in CH_3CN Solution

		PL at room temperature[c]				PL at 77 K[d]
	absorption λ [nm] (ε [$\times 10^4$ M^{-1} cm^{-1}])[b]	λ [nm]	Φ_p (τ [μs])	k_r [10^5 s^{-1}]	k_{nr} [10^6 s^{-1}]	λ [nm]
1[a]	256 (4.36), 385 (0.47), 411 (0.31)	480, 509	0.03 (0.18)	1.7	5.2	478, 512, 548
2	257 (4.06), 380 (0.46), 412 (0.31)	480, 507	0.008 (0.05)	1.6	20	471, 506, 538
3	253 (4.15), 380 (0.45), 410 (0.29)	476, 506	0.32 (2.0)	1.6	0.34	475, 511, 543

[a]Data of complex **1** were cited from ref 25. [b]In CH_3CN solution (1×10^{-5} M). ε denotes the molar extinction coefficient. [c]In degassed CH_3CN (1×10^{-5} M) solution. [d]In CH_3CN glass.

dx.doi.org/10.1021/ic2021325 | Inorg. Chem. 2012, 51, 4502–4510

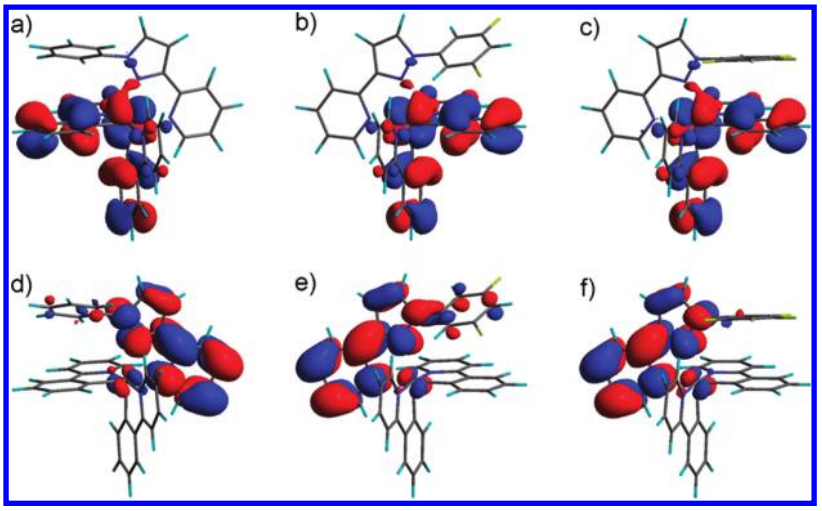

Figure 3. Optimized geometries and calculated molecular surfaces of complexes **1**−**3**. (a−c): HOMOs of complexes **1**−**3**. (d −f): LUMOs of complexes **1**−**3**. All the MO surfaces correspond to an isocontour value of |Ψ| = 0.025.

overestimated, as always observed when the B3LYP functional is adopted.[46] Figure 3 depicts the optimized geometries and calculated molecular surfaces of complexes **1**−**3** on the ground states. As shown in Figure 3, the pendant phenyl rings on the ancillary ligands stack to the phenyl rings of the ppy ligands, with dihedral angles of 25.4°, 24.9°, and 10.4° between least-squares planes for complexes **1**, **2**, and **3**, respectively, and centroid-centroid distances of 4.06 Å, 3.92 Å and 3.68 Å for complexes **1**, **2**, and **3**, respectively. Theoretical calculations reveal that, upon fluorinating the pendant phenyl ring, the intramolecular phenyl−phenyl stacking becomes more parallel and closer.

To compare the intramolecular $\pi-\pi$ stacking interactions in complexes **1**−**3**, single-point energy calculations were performed on the complexes with varied dihedral angles (Φ) between the two stacking phenyl rings. The Φ values are varied by rotating the pendant phenyl rings on the ancillary ligands. The calculated single-point energies ΔE (with respect to S_0) of complexes **1**−**3** are plotted versus Φ in Figure 4. Detailed ΔE

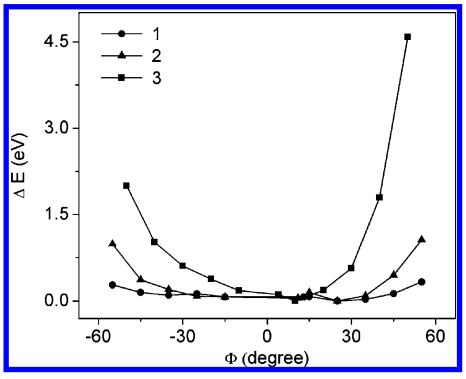

Figure 4. Variation of calculated single-point energies (ΔE, with respect to S_0) with dihedral angles (Φ) between the two stacking phenyl rings for complexes **1**−**3**.

values can be found in the Supporting Information (Table S2). It should be noted that, in complexes **1**−**3**, the pendant phenyl rings cannot stack absolutely parallel (Φ = 0°) to the phenyl rings of the ppy ligands. By rotating the pendant phenyl rings, the accessible smallest Φ values are 13°, 11°, and 4° for complexes **1**, **2**, and **3**, respectively. Starting from the S_0 geometry (where ΔE = 0), the Φ values are gradually increased with a step of 10°. Starting from the S_0 geometry, the Φ values are reduced to the smallest values and then gradually increased with a step of 10°. In the latter case, the Φ values are minus so that they can be distinguished from those in the former case. In both cases, the calculated single-point energies are increased with respect to S_0 ($\Delta E > 0$). As shown in Figure 4, within an energy well of the same depth, the Φ for complex **3** spans in a much narrower range as compared to those for complexes **1** and **2**. For example, within an energy well of 0.2 eV, the Φ can vary between 45° ∼ −45° for complex **1**, 35° ∼ −35° for complex **2** and 20° ∼ −10° for complex **3**. Single-point energy calculations reveal that, compared to the pendant phenyl or 3,5-difluorophenyl rings in complexes **1** and **2**, the pendant pentafluorophenyl ring in complex **3** cannot swing by a large degree, which agrees with the significantly reinforced intramolecular $\pi-\pi$ stacking interaction in complex **3**.

As shown in Figure 3, for complexes **1**−**3**, the highest occupied molecular orbitals (HOMOs) reside on the iridium ions and the phenyl rings of the ppy ligands, and the lowest unoccupied molecular orbitals (LUMOs) reside on the pyridine-pyrazole moieties of the ancillary ligands. The HOMO-1, LUMO+1, and LUMO+2 orbitals of complexes **1**−**3** reside mainly on the ppy ligands (Supporting Information, Figure S2).

To ascertain the character of excited states, TDDFT calculations were conducted on the basis of the optimized S_0 geometries. Table 4 summarizes the lowest three singlet and triplet states, together with the calculated oscillator strengths (f) for the excitations. More singlet−singlet transitions can be found in the Supporting Information (Table S4). The calculated f values for the triplet excitations are zero because of the neglect of the spin−orbit coupling in TDDFT calculations. In phosphorescent heave-metal complexes, the spin−orbit coupling makes the spin-forbidden triplet excitations partially allowable and the real oscillator strengths for the triplet excitations should be positive.

As shown in Table 4, for the three complexes, the S_1, S_2, and S_3 states arise mainly from the HOMO→LUMO, HOMO→LUMO+1, and HOMO→LUMO+2 excitations, respectively, except that, for complex **3**, the HOMO-1→LUMO excitation also has a large contribution to the S_3 state. For the three

dx.doi.org/10.1021/ic2021325 | Inorg. Chem. 2012, 51, 4502−4510

Table 4. Selected Singlet and Triplet States of Complexes 1−3 Calculated from a TDDFT Approach

	states	E [eV]	f^a	dominant excitations[b]
1	S_1	2.604	0.0008	H → L (100%)
	S_2	3.038	0.0339	H → L+1 (100%)
	S_3	3.182	0.0004	H → L+2 (100%)
	T_1	2.594	0	H → L (97%)
	T_2	2.700	0	H →L+1 (62%), H−1→L+2 (19%)
	T_3	2.772	0	H → L+2 (44%), H−1→L+1 (36%)
2	S_1	2.524	0.0001	H → L (100%)
	S_2	3.036	0.0281	H → L+1 (100%)
	S_3	3.165	0.0022	H → L+2 (95%)
	T_1	2.512	0	H → L (100%)
	T_2	2.704	0	H →L+1 (61%), H−1→L+2 (15%)
	T_3	2.769	0	H →L+2 (39%), H−1→L+1 (31%),
3	S_1	2.518	0.0002	H → L (100%)
	S_2	3.106	0.0361	H → L+1 (100%)
	S_3	3.216	0.0035	H−1 → L (41%), H → L+2 (53%)
	T_1	2.515	0	H → L (100%)
	T_2	2.737	0	H →L+1(66%), H−1 →L+2 (14%)
	T_3	2.791	0	H →L+2 (35%), H−1→L+1(33%)

[a]Calculated oscillator strengths. [b]H and L denote HOMO and LUMO, respectively; data in parentheses are the contributions of excitations.

complexes, the T_1 and T_2 states arise mainly from the HOMO → LUMO and HOMO → LUMO+1 excitations, respectively, while the T_3 states have large multiconfigurational character and arise mainly from HOMO→LUMO+2 and HOMO-1→LUMO+1 excitations. According to the distributions of the molecular orbitals, it can be concluded that the T_1 states have mixed ^{3}MLCT (Ir → F2phpzpy or F5phpzpy) and ^{3}LLCT (ppy → F2phpzpy or F5phpzpy) character; the T_2 and T_3 states have mixed ^{3}MLCT (Ir → ppy) and ppy-centered $^3\pi-\pi^*$ character. As revealed in the photophysical characterizations, the emission of complexes **1**−**3** exhibits strong ligand-centered $^3\pi-\pi^*$ character. It is thus deduced that the T_2 or T_3 states should have contributions to the emission for complexes **1**−**3**, that is, the ppy-centered $^3\pi-\pi^*$ states should contribute to the emission for complexes **1**−**3**. The previous research has shown that, for a blue-green-emitting cationic iridium complex with the lowest triplet states close-lying in energy, the emission in solution could occur from the T_4 state which had ligand-centered $^3\pi-\pi^*$ character.[45] For complexes **1**−**3**, the lowest three triplet states could also be close-lying in energy, as expected from the close-lying triplet excitation energies (Table 4). For complexes **1**−**3**, the emission could occur from the T_2 or T_3 states. However, quantitative analysis of the contribution of the T_2 and T_3 states to the emission is difficult to achieve because the calculated oscillator strengths for the triplet excitations are zero in the TDDFT calculations.

The lowest triplet states (T_1) of complexes **1**−**3** were optimized at UB3LYP levels with a spin multiplicity of 3 on the basis of the optimized S_0 geometries. Figure 5 shows the optimized geometries and spin density distributions on the T_1 states. The selected bond lengths and angles on the T_1 states are summarized in Table 5. As comparisons, the data on the singlet S_0 states are also listed. As shown in Figure 5, the spin densities of the T_1 states distribute on the phenyl rings of the ppy ligands, the iridium ions, and the ancillary ligands. The spin density distributions of the T_1 states have a good match with the topologies of HOMO and LUMO orbitals (Figure 3). This agrees with the TDDFT calculations which reveal that the T_1 states correspond to electron promotions from HOMO to LUMO orbitals.

As shown in Table 5, compared to the S_0 geometries, the geometries on the T_1 states exhibit a little contracted coordination, as revealed by the shortened metal−ligand bonds. In passing from the S_0 to the T_1 states, small structural changes are observed for the two ppy ligands, while significant structural changes are observed for the ancillary ligands. For complexes **1**−**3**, in passing from the S_0 to the T_1 states, the pendant phenyl rings on the ancillary ligands just show a small deviation, as revealed by the small changes (2−5°) of the dihedral angles (Φ) between the two stacking phenyl rings. For complex **3** on the T_1 state, the pendant pentafluorophenyl ring stacks to the phenyl ring of the ppy ligand, with a dihedral angle of 12° between least-squares planes and a centroid-to-centroid distance of 3.69 Å, indicating that the intramolecular $\pi-\pi$ stacking interaction remains on the T_1 state.

For complexes **1**−**3**, the pyridine-pyrazole skeletons are more twisted on the T_1 states, as revealed by the increases (5−9°) of the dihedral angles (φ) between the pyridine and pyrazole rings on the ancillary ligands (Table 5). For complexes **1** and **2**, in passing from the S_0 to the T_1 states, a significant structural change should be the deviation of the pyrazole moieties on the ancillary ligands, as revealed by the large changes (10−20°) of the dihedral angles (θ) between the pendant phenyl rings and the pyrazole rings on the ancillary ligands (Table 5). For complex **3**, the deviation of the pyrazole moiety on the T_1 state is small, as revealed by the small change (5°) of the θ value in passing from the S_0 to the T_1 states. Among the three complexes, complex **3** shows the smallest changes in θ, φ, and Φ values, indicating that complex **3** has the smallest structural changes between the S_0 and the T_1 states.

It is believed that, in complex **3**, the significantly reinforced intramolecular $\pi-\pi$ stacking interaction restricts the structure of the complex on both the ground and the excited states, which prevents large structural relaxations on the excited states. For complex **3**, the small structural changes between the ground and the excited states would significantly attenuate the nonradiative deactivation of the excited-states and increase the PL efficiency of the complex in solution.[24] For complex **2**,

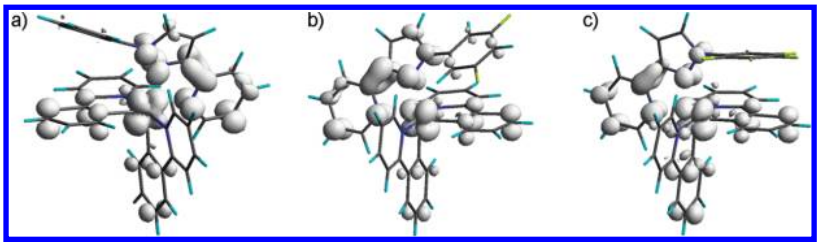

Figure 5. Spin density distribution (0.004 e bohr^{-3}) on the T_1 states for (a) complex **1**; (b) complex **2**; (c) complex **3**.

dx.doi.org/10.1021/ic2021325 | Inorg. Chem. 2012, 51, 4502−4510

Table 5. Selected Bond Lengths (Å) and Angles (deg) Calculated for Complexes 1−3 on the S_0 and T_1 States

	states	Ir−C(ppy)	Ir−N(ppy)	Ir−N(N∧N)	C−C[a]	θ[b]	φ[c]	Φ[d]	d[e]
1	S_0	2.014/2.025	2.083/2.082	2.247/2.288	1.463	61	3.7	25	4.06
	T_1	2.006/1.989	2.081/2.082	2.233/2.230	1.413	50	13	27	4.02
2	S_0	2.011/2.025	2.082/2.081	2.251/2.298	1.464	53	8.7	25	3.92
	T_1	2.009/1.993	2.082/2.074	2.218/2.256	1.414	33	16	30	3.87
3	S_0	2.015/2.024	2.084/2.085	2.251/2.258	1.464	83	2.4	10	3.68
	T_1	1.984/1.997	2.075/2.081	2.238/2.240	1.426	78	7.0	12	3.69

[a]C−C bond connecting the pyridine and pyrazole rings on the ancillary ligand. [b]Dihedral angle between the pendant phenyl ring and the pyrazole ring on the ancillary ligand. [c]Dihedral angle between the pyridine and pyrazole rings on the ancillary ligand. [d]Dihedral angle between the two stacking phenyl rings. [e]Centroid-centroid distance between the two stacking phenyl rings.

substituting the pendant phenyl ring with two fluorine atoms is insufficient to guarantee a strong enough intramolecular $\pi-\pi$ stacking interaction that can prevent large structural relaxation on the excited states. For complex **2**, the structural changes between the ground and the excited states are still large, and complex **2** shows a low PL efficiency in solution.

CONCLUSION

By fluorinating the pendant phenyl ring on the ancillary ligand in $[Ir(ppy)_2(phpzpy)]PF_6$, two new complexes, $[Ir(ppy)_2(F2phpzpy)]PF_6$ and $[Ir(ppy)_2(F5phpzpy)]PF_6$, have been synthesized and compared to the parent complex $[Ir(ppy)_2(phpzpy)]PF_6$. Upon fluorination, the pendant phenyl rings on the ancillary ligands stack more parallel and closer to the phenyl rings of the ppy ligands, with $[Ir(ppy)_2(F5phpzpy)]PF_6$ exhibiting a significantly reinforced intramolecular face-to-face $\pi-\pi$ stacking interaction and a high luminescent efficiency in solution. Theoretical calculations revealed that, for $[Ir(ppy)_2(F5phpzpy)]PF_6$, the intramolecular $\pi-\pi$ stacking interaction remains on both the ground and the excited triplet states. The research demontrates an efficient approach to control the intramolecular $\pi-\pi$ stacking interaction in phosphorescent iridium complexes, which opens a new avenue to modulate the structures and photophysical properties of the complexes.

ASSOCIATED CONTENT

Supporting Information

PL spectra of complexes **1**−**3** in 5% doped PMMA films and neat films (Figure S1). Distributions of HOMO-1, LUMO+1, and LUMO+2 on the complexes (Figure S2). Comparisons of the calculated and experimental absorption spectra (Figure S3). Selected bond lengths and angles on the ground states from DFT (Table S1). Calculated single-point energies of complexes **1**−**3** (Table S2). Cartesian coordinates of all the optimized S_0 and T_1 geometries (Table S3). The first thirty singlet−singlet transitions from TDDFT for complexes **1**−**3** (Table S4). The Crystallographic Information (CIF) Files of complexes **2** and **3**. This material is available free of charge via the Internet at http://pubs.acs.org.

AUTHOR INFORMATION

Corresponding Author

*Phone: 86-10-62779988. Fax: 86-10-62795137. E-mail: qiuy@mail.tsinghua.edu.cn (Y.Q.), duanl@mail.tsinghua.edu.cn (L.D.).

Notes

The authors declare no competing financial interest.

ACKNOWLEDGMENTS

We would like to thank the National Key Basic Research and Development Program of China (Grant 2009CB930602), the National High Technology Research and Development Program of China (Grant 2011AA03A110), and the National Natural Science Foundation of China (Grants 50990060 and 51073089) for financial support.

REFERENCES

(1) Pei, Q. B.; Yu, G.; Zhang, C.; Yang, Y.; Heeger, A. J. *Science* **1995**, *269*, 1086.
(2) Matyba, P.; Maturova, K.; Kemerink, M.; Robinson, N. D.; Edman, L. *Nat. Mater.* **2009**, *8*, 672.
(3) Slinker, J. D.; Gorodetsky, A. A.; Lowry, M. S.; Wang, J. J.; Parker, S.; Rohl, R.; Bernhard, S.; Malliaras, G. G. *J. Am. Chem. Soc.* **2004**, *126*, 2763.
(4) Slinker, J. D.; Rivnay, J.; Moskowitz, J. S.; Parker, J. B.; Bernhard, S.; Abruna, H. D.; Malliaras, G. G. *J. Mater. Chem.* **2007**, *17*, 2976.
(5) Plummer, E. A.; van Dijken, A.; Hofstraat, H. W.; De Cola, L.; Brunner, K. *Adv. Funct. Mater.* **2005**, *15*, 281.
(6) He, L.; Duan, L.; Qiao, J.; Zhang, D. Q.; Dong, G. F.; Wang, L. D.; Qiu, Y. *Org. Electron.* **2009**, *10*, 152.
(7) He, L.; Duan, L. A.; Qiao, J. A.; Zhang, D. Q.; Wang, L. D.; Qiu, Y. *Org. Electron.* **2010**, *11*, 1185.
(8) Bolink, H. J.; Coronado, E.; Costa, R. D.; Lardies, N.; Orti, E. *Inorg. Chem.* **2008**, *47*, 9149.
(9) He, L.; Duan, L.; Qiao, J.; Wang, R. J.; Wei, P.; Wang, L. D.; Qiu, Y. *Adv. Funct. Mater.* **2008**, *18*, 2123.
(10) Su, H. C.; Chen, H. F.; Fang, F. C.; Liu, C. C.; Wu, C. C.; Wong, K. T.; Liu, Y. H.; Peng, S. M. *J. Am. Chem. Soc.* **2008**, *130*, 3413.
(11) He, L.; Qiao, J.; Duan, L.; Dong, G. F.; Zhang, D. Q.; Wang, L. D.; Qiu, Y. *Adv. Funct. Mater.* **2009**, *19*, 2950.
(12) Rothe, C.; Chiang, C. J.; Jankus, V.; Abdullah, K.; Zeng, X. S.; Jitchati, R.; Batsanov, A. S.; Bryce, M. R.; Monkman, A. P. *Adv. Funct. Mater.* **2009**, *19*, 2038.
(13) He, L.; Duan, L. A.; Qiao, J. A.; Dong, G. F.; Wang, L. D.; Qiu, Y. *Chem. Mater.* **2010**, *22*, 3535.
(14) Mydlak, M.; Bizzarri, C.; Hartmann, D.; Sarfert, W.; Schmid, G.; De Cola, L. *Adv. Funct. Mater.* **2010**, *20*, 1812.
(15) Yang, C. H.; Beltran, J.; Lemaur, V.; Cornil, J.; Hartmann, D.; Sarfert, W.; Frohlich, R.; Bizzarri, C.; De Cola, L. *Inorg. Chem.* **2010**, *49*, 9891.
(16) Bolink, H. J.; Coronado, E.; Costa, R. D.; Orti, E.; Sessolo, M.; Graber, S.; Doyle, K.; Neuburger, M.; Housecroft, C. E.; Constable, E. C. *Adv. Mater.* **2008**, *20*, 3910.
(17) Graber, S.; Doyle, K.; Neuburger, M.; Housecroft, C. E.; Constable, E. C.; Costa, R. D.; Orti, E.; Repetto, D.; Bolink, H. J. *J. Am. Chem. Soc.* **2008**, *130*, 14944.
(18) Costa, R. D.; Orti, E.; Bolink, H. J.; Graber, S.; Housecroft, C. E.; Neuburger, M.; Schaffner, S.; Constable, E. C. *Chem. Commun.* **2009**, 2029.
(19) Costa, R. D.; Orti, E.; Bolink, H. J.; Graber, S.; Housecroft, C. E.; Constable, E. C. *Adv. Funct. Mater.* **2010**, *20*, 1511.

(20) Costa, R. D.; Orti, E.; Bolink, H. J.; Graber, S.; Housecroft, C. E.; Constable, E. C. *J. Am. Chem. Soc.* **2010**, *132*, 5978.
(21) Costa, R. D.; Orti, E.; Bolink, H. J.; Graber, S.; Housecroft, C. E.; Constable, E. C. *Chem. Commun.* **2011**, *47*, 3207.
(22) Hunter, C. A.; Sanders, J. K. M. *J. Am. Chem. Soc.* **1990**, *112*, 5525.
(23) Sinnokrot, M. O.; Sherrill, C. D. *J. Phys. Chem. A* **2006**, *110*, 10656.
(24) Costa, R. D.; Monti, F.; Accorsi, G.; Barbieri, A.; Bolink, H. J.; Orti, E.; Armaroli, N. *Inorg. Chem.* **2011**, *50*, 7229.
(25) He, L.; Duan, L.; Qiao, J.; Zhang, D. Q.; Wang, L. D.; Qiu, Y. *Chem. Commun.* **2011**, *47*, 6467.
(26) Battaglia, M. R.; Buckingham, A. D.; Williams, J. H. *Chem. Phys. Lett.* **1981**, *78*, 420.
(27) Williams, J. H. *Acc. Chem. Res.* **1993**, *26*, 593.
(28) Patrick, C. R.; Prosser, G. S. *Nature* **1960**, *187*, 1021.
(29) Coates, G. W.; Dunn, A. R.; Henling, L. M.; Dougherty, D. A.; Grubbs, R. H. *Angew. Chem., Int. Ed. Engl.* **1997**, *36*, 248.
(30) Babudri, F.; Farinola, G. M.; Naso, F.; Ragni, R. *Chem. Commun.* **2007**, 1003.
(31) Tang, M. L.; Bao, Z. A. *Chem. Mater.* **2011**, *23*, 446.
(32) Melhuish, W. H. *J. Phys. Chem.* **1961**, *65*, 229.
(33) Palsson, L. O.; Monkman, A. P. *Adv. Mater.* **2002**, *14*, 757.
(34) Becke, A. D. *J. Chem. Phys.* **1988**, *88*, 2547.
(35) Lee, C. T.; Yang, W. T.; Parr, R. G. *Phys. Rev. B* **1988**, *37*, 785.
(36) Becke, A. D. *J. Chem. Phys.* **1993**, *98*, 5648.
(37) Francl, M. M.; Pietro, W. J.; Hehre, W. J.; Binkley, J. S.; Gordon, M. S.; Defrees, D. J.; Pople, J. A. *J. Chem. Phys.* **1982**, *77*, 3654.
(38) Hay, P. J.; Wadt, W. R. *J. Chem. Phys.* **1985**, *82*, 299.
(39) Frisch, M. J.; Trucks, G. W.; Schlegel, H. B.; Scuseria, G. E.; Robb, M. A.; Cheeseman, J. R.; Montgomery, J., J. A.; Vreven, T.; Kudin, K. N.; Burant, J. C.; Millam, J. M.; Iyengar, S. S.; Tomasi, J.; Barone, V.; Mennucci, B.; Cossi, M.; Scalmani, G.; Rega, N.; Petersson, G. A.; Nakatsuji, H.; Hada, M.; Ehara, M.; Toyota, K.; Fukuda, R.; Hasegawa, J.; Ishida, M.; Nakajima, T.; Honda, Y.; Kitao, O.; Nakai, H.; Klene, M.; Li, X.; Knox, J. E.; Hratchian, H. P.; Cross, J. B.; Bakken, V.; Adamo, C.; Jaramillo, J.; Gomperts, R.; Stratmann, R. E.; Yazyev, O.; Austin, A. J.; Cammi, R.; Pomelli, C.; Ochterski, J. W.; Ayala, P. Y.; Morokuma, K.; Voth, G. A.; Salvador, P.; Dannenberg, J. J.; Zakrzewski, V. G.; Dapprich, S.; Daniels, A. D.; Strain, M. C.; Farkas, O.; Malick, D. K.; Rabuck, A. D.; Raghavachari, K.; Foresman, J. B.; Ortiz, J. V.; Cui, Q.; Baboul, A. G.; Clifford, S.; Cioslowski, J.; Stefanov, B. B.; Liu, G.; Liashenko, A.; Piskorz, P.; Komaromi, I.; Martin, R. L.; Fox, D. J.; Keith, T.; Al-Laham, M. A.; Peng, C. Y.; Nanayakkara, A.; Challacombe, M.; Gill, P. M. W.; Johnson, B.; Chen, W.; Wong, M. W.; Gonzalez, C.; Pople, J. A. *Gaussian 03*, Revision B.05; Gaussian, Inc.: Wallingford, CT, 2004.
(40) Colombo, M. G.; Hauser, A.; Gudel, H. U. *Inorg. Chem.* **1993**, *32*, 3088.
(41) Colombo, M. G.; Brunold, T. C.; Riedener, T.; Gudel, H. U.; Fortsch, M.; Burgi, H. B. *Inorg. Chem.* **1994**, *33*, 545.
(42) You, Y.; Huh, H. S.; Kim, K. S.; Lee, S. W.; Kim, D.; Park, S. Y. *Chem. Commun.* **2008**, 3998.
(43) Shan, G. G.; Zhu, D. X.; Li, H. B.; Li, P.; Su, Z. M.; Liao, Y. *Dalt. Trans.* **2011**, *40*, 2947.
(44) Shan, G. G.; Zhang, L. Y.; Li, H. B.; Wang, S.; Zhu, D. X.; Li, P.; Wang, C. G.; Su, Z. M.; Liao, Y. *Dalt. Trans.* **2012**, *41*, 523.
(45) Bolink, H. J.; Cappelli, L.; Cheylan, S.; Coronado, E.; Costa, R. D.; Lardies, N.; Nazeeruddin, M. K.; Orti, E. *J. Mater. Chem.* **2007**, *17*, 5032.
(46) Nozaki, K.; Takamori, K.; Nakatsugawa, Y.; Ohno, T. *Inorg. Chem.* **2006**, *45*, 6161.
(47) Neve, F.; Crispini, A.; Campagna, S.; Serroni, S. *Inorg. Chem.* **1999**, *38*, 2250.

NOTE ADDED AFTER ASAP PUBLICATION

This paper was published on the Web on March 30, 2012. An additional reference was added to the paper, and the corrected version was reposted on April 5, 2012.